Influence of Particle Charging on the Fume Formation Process in Arc Welding†

TASHIRO Shinichi*, MURPHY B. Anthony, TANAKA Manabu*****

Abstract

In order to clarify the influence of electrostatic forces caused by charging of particles on the coagulation process in fume formation in arc welding, a previously-developed fume formation model has been modified to consider the influence of charging, for both local thermodynamic equilibrium (LTE) and non-LTE conditions. The model takes into account formation of the particles from metal vapour by nucleation, growth of the particles by condensation of metal vapour, and coagulation of the particles by collisions to form secondary particles. Results have been obtained for both ballistic and Brownian motion of the particles. It was found that the growth of secondary particles is suppressed when the average particle charge becomes significant, because charging of the particle hinders collisions among secondary particles through the strong repulsive electrostatic force. Furthermore, deviations from LTE strongly affect the coagulation process, because the increased electron density at a given gas temperature increases the charging of particles. Brownian motion leads to larger secondary particles, since the average particle speed is increased. The influence of Brownian motion and particle charging cancel each other to a large extent, particularly when deviations from LTE are considered.

KEY WORDS: (Fume), (Arc welding), (Charging), (Simulation)

1. Introduction

In arc welding, high-temperature metal vapour is generated by evaporation of molten metal; depending on the type of arc welding, this can include the molten tip of the welding wire, the droplets and the weld pool [1,2]. The metal vapour is cooled rapidly as it diffuses to the fringes of the arc. Metal nanoparticles, with sizes in the range 1 nm to 100 nm, are formed through nucleation from the metal vapour, and grow through condensation of metal vapour; we call these the primary particles. Some of these particles collide and produce secondary particles, with sizes up to over 1 μm. The particles have the appearance of smoke, which ascends from the arc and is known as welding fume [3].

Inhalation of welding fume is a significant occupational health problem. The size of the fume particles gives them a high probability of deposition in parts of the lungs where rapid clearance mechanisms are not effective. Further, certain metals, such as chromium (particularly hexavalent chromium) and nickel are of particular concern when inhaled [4].

Most papers on welding fume are concerned with the chemical composition and generation rate of the fume for consumable electrode welding methods, such as gas metal arc (GMA) and shielded metal arc (SMA) welding, because of their widespread use in manufacturing industries. For example, Kobayashi *et al* observed fume generation in SMA welding by employing a high-speed video camera. It was qualitatively explained that metal vapour was produced in the lower part of the arc column, and generated fume due to rapid cooling, together with condensation and oxidation. They also showed that the amount of metal vapour produced from the droplet was greater than that from the weld pool [3]. Jenkins *et al* measured the chemical composition of fume in SMA and GMA welding by energy dispersive spectroscopy (EDS) [5]. Bosworth *et al* discussed the influence of droplet size on the fume generation rate in GMA welding [6]. The research on welding fume has been almost exclusively confined to experimental observations, sometimes combined with engineering calculations (e.g. [7]). There has been little theoretical research directed towards clarifying the mechanism of fume formation; this requires a quantitative investigation, taking into account of the interactions between the electrode, the arc and the weld pool. In the cases of GMA and SMA welding, this is a particularly complex problem because of the formation of metal droplets from the electrode and their transfer to the

† Received on July 8, 2013
* Assistant professor
** CSIRO Materials Science and Engineering
*** Professor

Transactions of JWRI is published by Joining and Welding Research Institute, Osaka University, Ibaraki, Osaka 567-0047, Japan

weld pool; as a consequence, the interactions are not fully understood.

Theoretical research is more advanced in the field of industrial production of nanoparticles. Many researchers have reported numerical simulations clarifying the nanoparticle formation mechanism [8]. However, the particle shape is usually spherical in industrial processes, so little effort has been made to calculate particle morphologies. For example, Watanabe *et al* investigated a series of processes, from evaporation of powder by a thermal plasma, to nucleation and condensation in the quench region, for production of nanoparticles in an inductively-coupled plasma (ICP). The model assumed that all the particles were spherical, so the shape of the nanoparticles could not be investigated [9]. Shigeta and Watanabe extended this work to take into account coagulation of the primary particles, but the assumption of spherical particles was retained [10].

Schmid *et al* proposed a model of aggregate structure formation in aerosol processes that took into account the shape of secondary particles formed in the coagulation process, but this model was not coupled with the nucleation and condensation processes [11]. We are not aware of investigations (apart from our earlier paper, discussed below) that have considered all the processes necessary for a full treatment of welding fume formation, i.e. formation of metal vapour, nucleation of the vapour to form nanoparticles, their growth by condensation, and the formation of secondary particles of arbitrary shape by coagulation of the nanoparticles.

Gas tungsten arc (GTA) welding is an attractive process to study in clarifying the fume formation mechanism because of its relative simplicity, in particular the absence of metal transfer, and the fact that the metal vapour originates from only the weld pool. Recently, numerical simulations treating the electrode, the arc, and the weld pool as a single system, and taking into account their mutual thermal and dynamic interactions, have allowed quantitative prediction of the temperature and flow in the weld pool [12]. Tanaka *et al* and Mori *et al* have further developed such models, and additionally predicted the formation of the metal vapour from the weld pool and its diffusion in the arc [13,14]. Recently, Tashiro *et al* investigated the full set of processes, from evaporation of metal vapour to fume formation from the metal vapour, by employing GTA and GMA arc simulation models coupled to a fume formation model. The latter consisted of a homogeneous nucleation model, a condensation model, and a particle coagulation model [15]. This allowed the fume formation process to be visualized, and the mechanisms to be theoretically clarified, through numerical analysis.

However, there are many aspects of the fume formation mechanism in arc welding that are still not clear. For example, the influence of the electrostatic forces, caused by charging of particles, on the coagulation process requires clarification. **Figure 1** shows the electron density under the assumption of local thermodynamic equilibrium (LTE) as a function of temperature for argon, and a mixture of argon and 0.1% iron vapour. It is reasonable to assume that the influence of particle charging is negligible in the case of pure argon shielding gas, because the electron density is very small at the low temperatures (typically less than 3000 K) at which coagulation of particles occurs. However, the presence of even a small concentration of metal vapour greatly increases the electron density at low temperature because of the low ionization potential of metal atoms. As shown in **Figure 1**, the addition of 0.1% iron vapour increases the electron density by several orders of magnitude. This indicates that it is important to consider the influence of charging of particles in the formation of welding fume, since metal vapour is of course unavoidably present when fume is produced.

In addition, it is also likely that deviations from LTE affect the charging of particles. Under the LTE assumption, all species in the plasma have the same temperature, and chemical composition depends only on temperature. This assumption is applicable if the plasma has a high enough collision frequency between heavy species (neutral gas and ions) and electrons to allow full exchange of their thermal energy. It is generally considered to be valid for high-temperature plasmas with high electron density, such as occur in the centre of the arc column. However, it is less likely to apply to low-temperature regions such as the fringe of the arc column or the boundary regions close to the electrodes, due to the decreased energy exchange caused by the low electron density in these regions [16]. In this case, the electron temperature and the electron density become larger than those under LTE, because of the decrease in energy loss through collisions with heavy species. The increased electron density will enhance charging of particles.

Finally, the motion of the particles was previously calculated assuming ballistic trajectories between collisions with other particles [15]. In reality, once large particles are formed, they are subject to a high rate of collisions with gas-phase species, so a Brownian motion approach is more realistic.

This paper aims to clarify the influence of electrostatic forces, caused by charging of particles, and Brownian motion on the coagulation process through numerical simulation. This will be done using the welding fume formation model previously reported [15], with appropriate modifications.

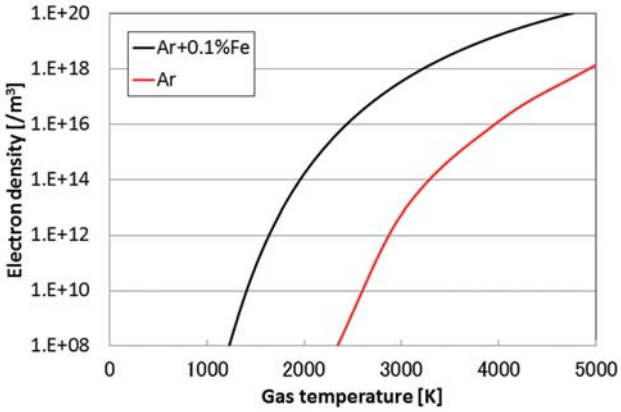

Fig. 1 Electron density, under the assumption of LTE, as a function of temperature for argon and a mixture of argon with 0.1 mol% iron vapour.

2. Fume formation model

The fume formation model consists of a homogeneous nucleation model, a condensation model and a coagulation model. **Figure 2** shows a summary of the fume formation model. The required input data for the fume formation model are the metal vapour partial pressure, the temperature and the cooling rate at a given nucleation site. These are calculated using a numerical model of the arc welding process that self-consistently includes the electrode, arc and weld pool, as described in [15].

In the fume formation model, the following steps are considered:

(1) Supersaturation of the iron vapour as the plasma gas cools;

(2) Formation of the primary particles by homogeneous nucleation of the iron vapour;

(3) Growth of the primary particles by condensation of iron vapour;

(4) Production of secondary particles by coagulation of the primary particles;

(5) Growth of the secondary particles by condensation and by coagulation.

The methods used in the model are considered in the following subsections.

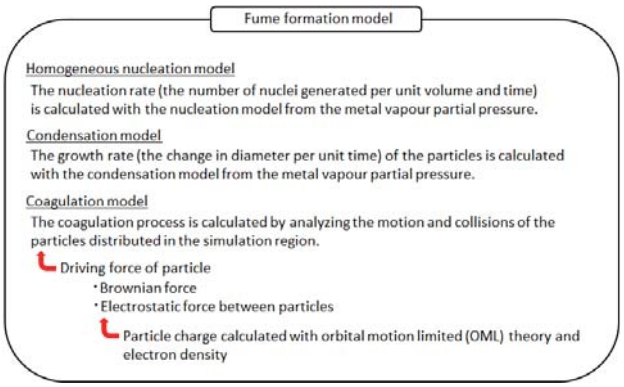

Fig. 2 Summary of the fume formation model.

2.1. Homogeneous nucleation model for primary particle formation

We employ Friedlander's liquid-drop model, in which all the nuclei are assumed to be generated in the liquid phase [17]. It is possible for homogeneous nucleation to occur if the degree of supersaturation exceeds 1. It is assumed that the nucleus with a critical diameter $d_{p\ \mathrm{cri}}$ is generated due to the nucleation. The critical diameter is the smallest nucleus diameter for which a stable particle can exist, and is given by

$$d_{p\ \mathrm{cri}} = \frac{4\sigma_p v_1}{kT \ln S} \tag{1}$$

where σ_p is surface tension, v_1 is the volume of the iron atom, k is the Boltzmann constant, T is the gas temperature and S is the degree of supersaturation. The homogeneous nucleation rate J, which is the number of nuclei generated per unit volume and time, is given by [18]:

$$J = N \frac{\zeta n_1}{12} \sqrt{\frac{\Theta}{2\pi}} \exp\left[-\frac{4\Theta^3}{27(\ln S)^2} \right] \tag{2}$$

where n_1 is the number density of iron atoms and N is a normalization constant given by equation (3). The Brownian collision frequency function between iron atoms, ζ, is given by equation (4), which is applicable if the Knudsen number is greater than 10; for the conditions considered here, its value is at least 1000. The dimensionless surface energy Θ is given by equation (5).

$$N = n_s \exp\Theta \tag{3}$$

$$\zeta = 4\left(\frac{3v_1}{4\pi}\right)^{1/6} \sqrt{\frac{12kT}{\rho}} \tag{4}$$

$$\Theta = \frac{\sigma_p s_1}{k\ T} \tag{5}$$

where n_s is the iron atom number density in the saturated vapour and s_1 is the surface area of the iron atom.

2.2. Condensation model for primary and secondary particle growth

Particle growth by condensation of the metal vapour is described using an equation for the growth rate G, the change in diameter per unit time, which can be obtained from a material balance over the surface of the growing particle [19]:

$$G = \frac{4}{d_p}\frac{R_g}{R_c} D_g \left(X - X_s\right)\left\{\frac{1+K_n}{1+1.7K_n+1.333K_n^2}\right\} \quad (6)$$

where d_p is the particle diameter, R_g and R_c are respectively the molar densities of the gas phase and the condensed phase, X is the metal vapour mole fraction, X_s is the metal vapour mole fraction under saturation conditions, D_g is the diffusion coefficient, defined as $\lambda\overline{v}/3$, where λ is mean free path of iron atoms and $\overline{v}$ is mean speed of iron atoms [20], and K_n is the Knudsen number, defined as $K_n=\lambda/(d_p/2)$.

2.3. Coagulation model for secondary particle formation

The primary particles generated by nucleation grow through not only the condensation of iron atoms, but also through coagulation as a consequence of collisions between particles. The coagulation process is calculated by analyzing the motion and collisions of particles distributed in the simulation region. A two-dimensional simulation region for the coagulation model is defined to reduce the computation time to a reasonable level. The size of the region is determined from the number density of primary particles such that 500 particles are included. The three-dimensional number density of primary particles determined from the primary particle model is converted into the two-dimensional number density by raising it to the power of 2/3. Secondary particles with a huge range of shapes and sizes are formed in arc welding, because the formation process is highly stochastic. However, only several or several tens of secondary particles are analyzed in the simulation due to limitations imposed by the computational resources; nevertheless these serve as representative examples of the particle morphologies produced.

Coagulation occurs by collision through ballistic motion for particles of dimensions much smaller than the mean free path of gas molecules. For particles of dimensions larger than the mean free path, the particle collisions are dominated mainly by Brownian motion of particles [21]. Although the mean free path is approximately several hundred nanometres in the temperature range in which coagulation occurs in case of GTA welding, the size of the fume particles changes from the order of nanometres immediately after nucleation, to a maximum of the order of micrometres after coagulation. Therefore, it is necessary to investigate coagulation processes for both types of motion.

When nucleation occurs, a primary particle is posted at a random position in the region and an initial velocity with a random direction is given to the particle. The initial velocity is discussed in section 2.3.1. The sum of the particles momentums is conserved in a collision. If the particles are at temperatures above the melting point when they collide, they are assumed to coalesce into a spherical particle, conserving their volumes. In other cases, they agglomerate; i.e., they attach to each other at the point of contact, forming a chain-like structure. A particle that escapes through a boundary of the computational region is injected at the opposite boundary with the same velocity vector.

2.3.1. Particle motion

In the case of ballistic motion, the initial velocities of the particles are set equal to the thermal velocity at the nucleation temperature. In the case of Brownian motion, the driving force of the particle (the Brownian force) is calculated using the following equation [22]:

$$F_B = \xi\sqrt{\frac{6\pi d_p \mu k T}{\Delta t C_c}} \quad (7)$$

where μ is the viscosity, Δt is the magnitude of the time step, C_c is the Cunningham correction to the Stokes drag, and ξ is a Gaussian random number with zero mean and unit variance. The random direction of the Brownian force is accounted for by evaluating both the x and y components of F_B at each time step using independent values of ξ in the two directions.

2.3.2. Charging of particles

Collision frequencies between particles and plasma charge carriers (ions and electrons) are calculated using orbital motion limited (OML) theory, which considers the interception of ions and electrons by a charged particle, accounting for the attraction or repulsion between charged collision partners [23]. For a particle with radius r_p and charge c, the electron collision frequency is determined from equation (8), and depends on the electron mass m_e, the electron density N_e and the electron temperature T_e. The attraction or repulsion factor α_e is calculated from equation (9) or (10), depending on the sign of the particle charge, and Φ_c is the particle surface potential, calculated according to equation (11); e is the electron charge.

$$\nu_e = \pi {r_p}^2 N_e \left(\frac{8kT_e}{\pi m_e}\right)^{\frac{1}{2}} \alpha_e \quad (8)$$

$$\alpha_e = \exp\left(\frac{e\Phi_c}{kT_e}\right) \quad (c<0) \quad (9)$$

$$\alpha_e = 1+\frac{e\Phi_c}{kT_e} \quad (c>0) \quad (10)$$

$$\Phi_c = \frac{ce}{4\pi\varepsilon_0 r_p} \quad (11)$$

The electron density in the case of an LTE plasma is calculated as a function of temperature and the mole fraction of metal vapour, using the method of minimization of the Gibbs free energy [2]. Typical results are shown in **figure 1**. In the case of non-LTE plasma

composition, for which the ratio of electron temperature to gas temperature $\theta = T_e/T > 1$, the electron density at a given electron temperature is determined from the LTE electron density using $N_e(T_e) = N_e(\theta T)$. For example, for $T_e = 3000$ K and $T = 1500$ K, the electron density corresponds to the LTE electron density for $T = 3000$ K. This approach is exact for a pure argon plasma, and a good approximation for an argon–iron plasma, as shown by the form of the two-temperature Saha equation [24].

Collision frequencies between positive ions and nanoparticles are calculated using equation (12), where E_0 is the ion energy, given by equation (13), and N_+ is the ion density (= N_e). Ions and particles are assumed to be in thermal equilibrium with the neutral gas molecules. The attraction or repulsion factor α_+ is given by equation (14) or (15) for collisions with negative or positive particles, respectively. For an uncharged nanoparticle, α_e and α_+ are set equal to 1.

$$\nu_+ = \pi {r_p}^2 N_+ \left(\frac{2E_0}{M_+}\right)^{\frac{1}{2}} \alpha_+ \tag{12}$$

$$E_0 = kT \tag{13}$$

$$\alpha_+ = 1 - \frac{e\Phi_c}{E_0} \quad (c < 0) \tag{14}$$

$$\alpha_+ = \exp\left(\frac{-e\Phi_c}{E_0}\right) \quad (c > 0) \tag{15}$$

From the above equations, the charge on each particle can be calculated. The electrostatic force between particles is obtained from

$$F_q = k_q \frac{q_1 q_2}{r^2} \tag{16}$$

where q_1 and q_2 are the charges on the particles, r is distance between particles and $k_q = 9.0 \times 10^9$ N m^{2}C^{-2} is a constant.

3. Calculation conditions

For the conditions investigated, nucleation occurs at temperatures around 2000 K. Therefore, the initial temperature for the calculation is set to 3000 K; this represents the temperature in the region of the arc plasma upstream from the region that fume formation occurs. The temperature decreases in 0.5 K steps until reaching the room temperature of 300 K. The homogeneous nucleation model, the condensation model and the coagulation model are solved in each temperature step. It is required to provide the metal vapour pressure and the cooling rate to the fume formation model as the initial conditions. The metal vapour pressure and the cooling rate are set to 169 Pa and 3.43×10^5 K s^{-1}, which are typical values for GTA welding [15]. The shielding gas and metal vapour are argon and iron, respectively.

In order to investigate influence of type of motion of the particles on the coagulation process, both ballistic motion and Brownian motion are considered. For both types of motion, the influence of particle charging is investigated. Further, to study the influence of of deviations from the LTE, the case of $T_e = 2T$ ($\theta = 2$) is investigated, in addition to the LTE case.

4. Results and discussion

4.1. Fume formation process in the case of ballistic motion without particle charging

To establish a base case, the fume formation process in case of ballistic motion, and neglecting the influence of particle charging, is investigated. In the absence of particle charging, the results are independent of electron density and therefore of the assumption of LTE.

Figure 3 shows the metal vapour partial pressure and the saturation pressure of iron as a function of temperature. The initial metal vapour partial pressure (at T = 3000 K) is set to 169 Pa, as noted in section 3. As the temperature decreases, the saturation pressure decreases, and supersaturation occurs at temperatures below 2200 K. Homogeneous nucleation of iron nanoparticles begins when the temperature falls to around 1700 K. It can be seen that metal vapour is rapidly consumed at the onset of homogeneous nucleation, due to the conversion of vapour to nanoparticles and the subsequent growth of the nanoparticles **by condensation.**

Figure 4 shows the dependence of the particle diameter distribution function on temperature. **Figure 5** shows four examples of the particle morphologies as the temperature decreases, at (a) 1670 K, (b) 1600 K, (c) 1500 K and (d) 300 K, at points denoted in **figure 4**. Nucleation commences at about 1700 K, with very small primary particles of diameter below 1 nm appearing. At 1670 K, the average particle speed is 212 m s^{-1}. Subsequently, the primary particles grow by condensation, and some of them coagulate to form secondary particles. The temperature of the particles is below the melting temperature of iron, so the particles agglomerate into chain-like structures, rather than coalescing into larger spheres. In particular, the diameters of the secondary particles rapidly increase as the temperature falls below 1650 K, due to agglomeration of the secondary particles. At 1600 K, the average speed has decreased to 41 m s^{-1} because of increase in particle weight. At 1500 K, all the primary particles have agglomerated, and the average speed has decreased to 0.8 m s^{-1}. Around this temperature, the maximum dimension of the secondary particles approaches 100 nm, and most of these tend to have pole-like shapes. When room temperature is reached, the secondary particles consist of 10 nm primary particles joined in a chain-like structure. The size of the largest secondary particle is

approximately 300 nm. The size of the primary particles is not uniform, because the amount of metal vapour that condenses on the primary particles depends on the nucleation temperature.

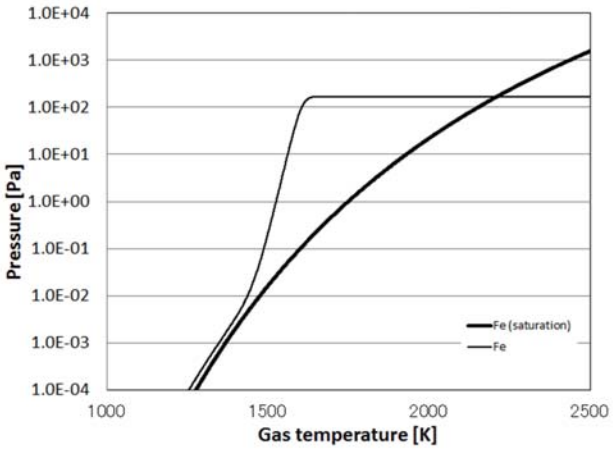

Fig. 3 Partial pressure and saturation pressure of iron vapour as a function of temperature in the case of ballistic motion neglecting particle charging.

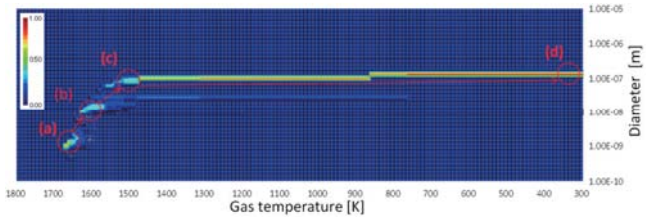

Fig. 4 Dependence of the particle diameter distribution function on temperature in the case of ballistic motion neglecting particle charging.

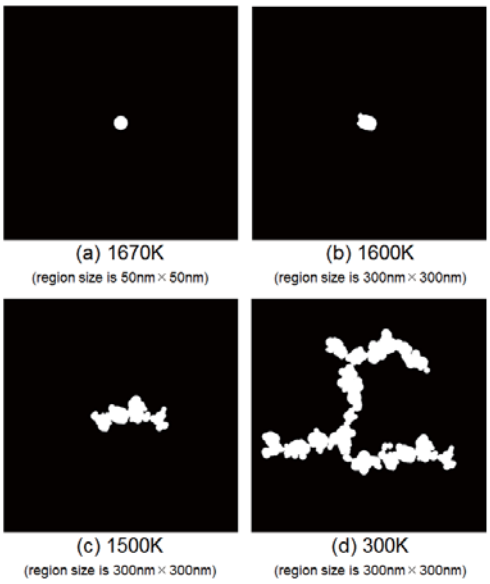

Fig. 5 Particle morphologies at four different temperatures, corresponding to those marked in **figure 4**.

4.2. Fume formation process in the case of Brownian motion without particle charging

The influence of assuming Brownian motion, rather than ballistic motion, of the particles is now considered. As in section 4.1, particle charging is neglected.

Figure 6 shows the dependence of the particle diameter distribution function on temperature. It was found that coagulation to form large secondary particles is favoured and the maximum diameter of the secondary particles reached approximately 100 nm at temperatures around 1570 K. The particle speed greatly increases in case of Brownian motion compared with that for ballistic motion. For example, the average particle speed reaches 161 m s^{-1} at 1570 K, despite the large particle diameter, because particles are continuously accelerated by the Brownian force. By the time the temperature has decreased to 1430 K, all the particles in the simulation region have coagulated to one large secondary particle.

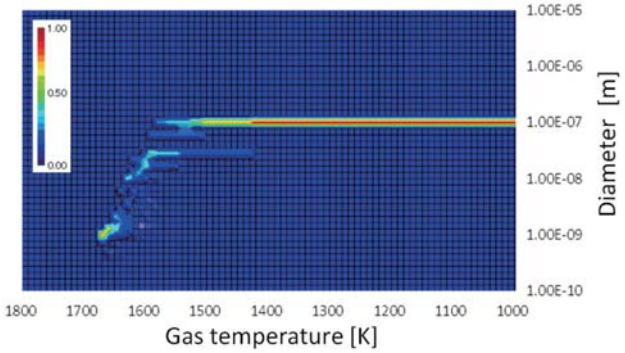

Fig. 6 Dependence of the particle diameter distribution function on temperature in the case of Brownian motion neglecting particle charging.

4.3. Fume formation process considering particle charging in the case of ballistic motion

We now consider the influence of particle charging on the coagulation process, assuming ballistic motion of the particles. We present results for both LTE and non-LTE plasmas.

Figure 7 shows the total particle charge in the simulation region and the average particle charge as function of temperature. **Figures 7** (a) and (b) correspond to results assuming LTE, and for $T_e = 2T$, respectively. It can be seen that the total particle charge reaches its maximum values at a temperature of about 1550 K. This is because particle charging stops at this temperature, since the vapour pressure of iron greatly decreases due to the consumption of the vapour by nucleation and condensation, and the electron density is many orders of magnitude lower when only argon is present (see **figure 1**). The total particle charge for $T_e = 2T$ is approximately 70 times larger than that for LTE conditions, because the collision frequency expressed by equation (8) is much higher due to the increase in electron temperature and electron density. Consequently, the average particle charge, which strongly affects the collision frequency between secondary particles through

the electrostatic force, is increased by a factor of 120, compared to the average particle charge for LTE conditions.

Figure 8 shows the dependence of the particle diameter distribution function on temperature for the same two cases considered in **figure 7**. Although the particle diameter distribution is largely unchanged by particle charging at temperatures above around 1600 K (cf **figure 4**), the growth of secondary particles is suppressed below this temperature, especially for the non-LTE case. This is because average particle charge greatly increases around 1600 K, as shown in **figure 7**, and this hinders collisions among secondary particles through the strong electrostatic repulsive force.

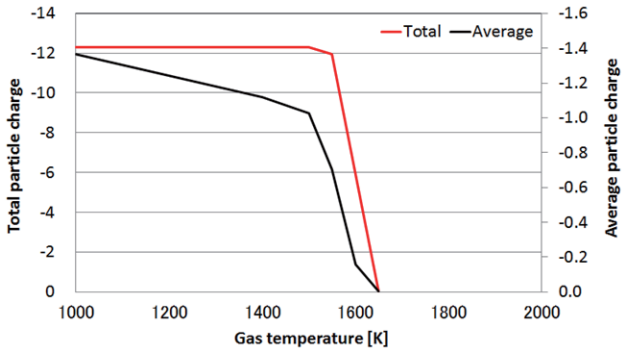

(a) Te = T

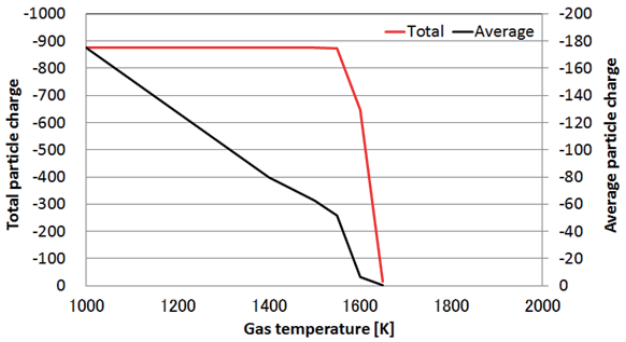

(b) Te = 2T

Fig. 7 Total particle charge and average particle charge as function of temperature in the case of ballistic motion, neglecting particle charging; (a) LTE, (b) $T_e = 2T$.

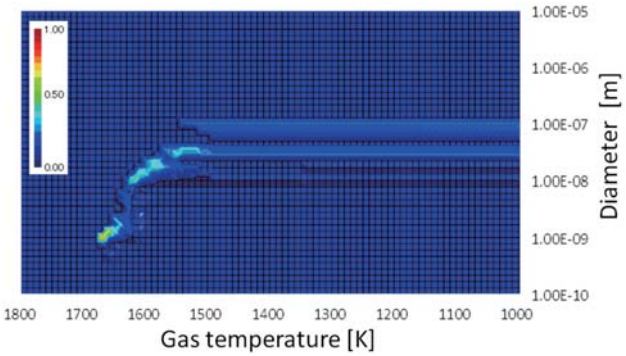

(a) Te = T

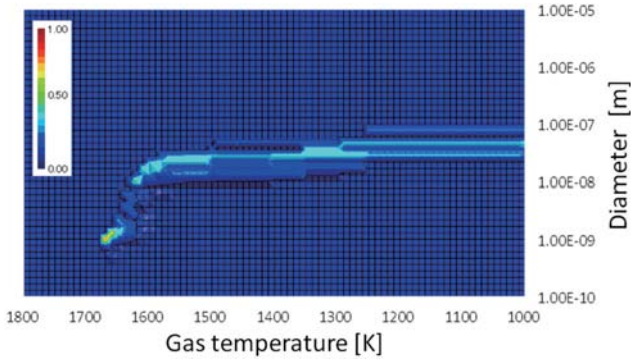

(b) Te = 2T

Fig. 8 Dependence of the particle diameter distribution function on temperature in the case of ballistic motion, taking into account the effects of particle charging; (a) LTE, (b) $T_e = 2T$.

4.4. Fume formation process considering particle charging in the case of Brownian motion

Finally, we consider the influence particle charging on the coagulation process, in the case of Brownian motion of the particles. As in section 4.3, we present results for both LTE and non-LTE plasmas.

Figure 9 shows the total particle charge in the simulation region and the average particle charge as function of temperature. **Figure 9** (a) and (b) correspond to results assuming LTE and for $T_e = 2T$, respectively. It was found that although the total particle charge is same as those shown for ballistic motion in **figures 7**(a) and (b) respectively, the average particle charge is larger because the diameter of the secondary particles increases. In **figure 9**(a), the average particle charge is equal to the total particle charge for temperatures below about 1400 K. This implies that all the particles in the simulation region are coagulated into one secondary particle. In the non-LTE case, this does not occur, because of the stronger repulsion between secondary particles, owing to the higher particle charging.

Figure 10 shows the dependence of the particle diameter distribution function on temperature. The same trends as shown in **figure 8** are apparent. Especially in the non-LTE case, the growth of secondary particles is suppressed at temperatures below approximately 1600 K, for which strong particle charging occurs.

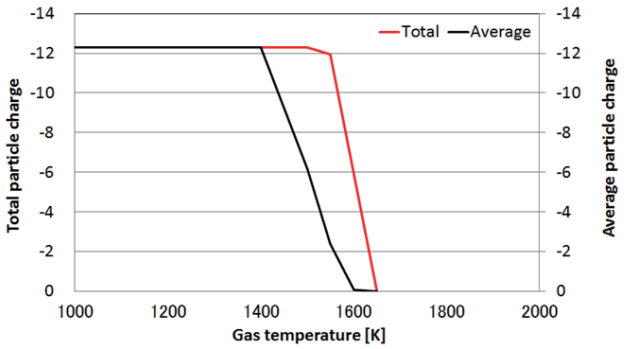

(a) Te = T

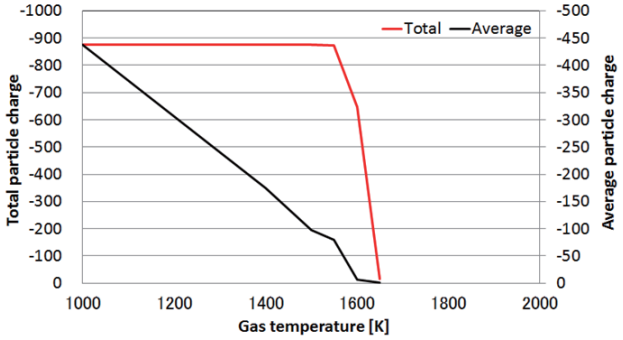

(b) Te = 2T

Fig. 9 Total particle charge and average particle charge as function of temperature in the case of Brownian motion; (a) LTE, (b) $T_e = 2T$.

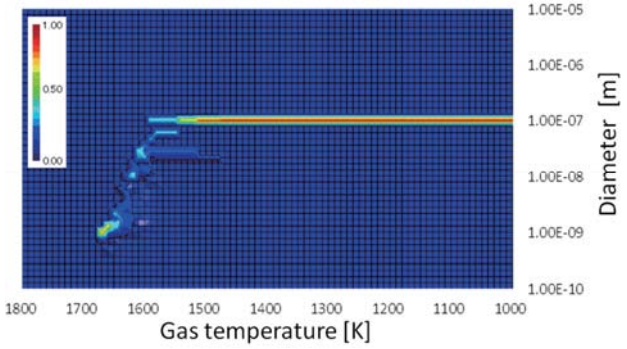

(b) Te = T

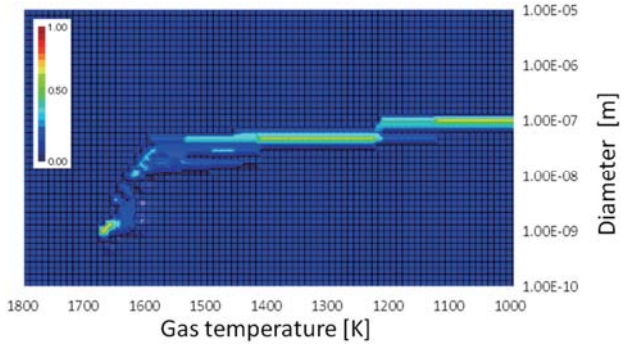

(b) Te = 2T

Fig. 10 Dependence of the particle diameter distribution function on temperature in the case of Brownian motion, taking into account the effects of particle charging; (a) LTE, (b) $T_e = 2T$.

4.5. Discussion

Brownian forces, and particle charging, have opposing effects on the coagulation of particles. Brownian forces increase the velocities of larger particles, making collisions and therefore coagulation more likely. Particle charging leads to negatively-charged particles, which repel each other electrostatically, making collisions and coagulation less likely. This is particularly the case when deviations from LTE are taken into account; this increases the electron density for a given gas temperature, and therefore the negative charge on particles.

As a consequence of these effects, taking into account Brownian motion and neglecting the influence of particle charging leads to larger secondary particles, compared to the base case (in which Brownian motion and particle charging are both neglected). Taking into account particle charging and neglecting the influence of Brownian motion, in contrast, leads to smaller secondary particles than in the base case. When both effects are included, the particle size is increased for LTE conditions, relative to the base case. For the most realistic assumptions (i.e. including Brownian motion, particle charging and deviations from LTE), the particle size distribution is similar to that obtained for the base case.

It is difficult to verify the predictions experimentally. As shown in our previous paper [15], the predicted particle size and chain-like morphology are consistent with those observed for fume particles collected during gas tungsten arc welding. We have shown here that, even though the different effects taken into account in the current work all have strong influences on the properties of the fume particles, when all effects are considered the particle size distribution is quite similar to that obtained in our previous paper [15].

In experimental studies, fume particles are collected from all points of the welding arc. This means that the particles collected will have been formed from regions with different metal vapour partial pressures, temperatures and quench rates. In this paper, our focus has been on determining the influence of different effects on the fume formation process, and therefore results have been obtained for a specific set of conditions, which apply at only a particular region of the arc plasma. It is not possible, particularly given the relatively small differences between the predictions of the improved model presented here and of the previous model, to test whether the agreement with experiment is improved. Nevertheless it is reasonable to conclude that the model presented here is more realistic, since the treatment of particle collisions and coagulation is significantly more sophisticated.

5. Conclusions

We have presented three important improvements to the welding fume formation model that was described in a previous paper [15]. These are taking into account Brownian motion of the larger fume particles, the influence of charging of the particles on their coagulation, and the influence of deviations from local thermodynamic equilibrium on the charging of the particles. All three improvements have significant influences on the particle distribution function.

1) The particle velocity is greatly increased when Brownian motion of the particles is taken into account. The secondary particle size is also larger, due to more frequent collisions between the particles.
2) When particle charging is taken into account, the growth of secondary particles is suppressed at lower

temperatures, because charging of the particle hinders collision among secondary particles through strong electrostatic repulsion.

3) Deviations from LTE further suppress the growth of secondary particles, by increasing the charging of particles as a consequence of the higher electron density.

The influence of particle charging, particularly when deviations from LTE are taken into account, tends to counteract the influence of Brownian motion. As a consequence, the predicted particle size distribution is fairly similar to that obtained in the previous work. Nevertheless, it is expected that the fume formation model is now significantly more reliable as a result of the improvements presented in this paper.

References

[1] Terasaki H, Tanaka M and Ushio M 2002 *Metall. Mater. Trans. A* **33** 1183− 8
[2] Murphy A B 2010 *J. Phys. D: Appl. Phys.* **43** 434001
[3] Antonini J M 2003 *Crit. Rev. Toxicol.* **33** 61–103
[4] Kobayashi M, Maki S, Hashimoto Y and Suga T 1980 *J. Japan Weld. Soc*. **49** 454–61
[5] Jenkins N T and Eagar T W 2005 *Weld. J.* **84** 87s–93s
[6] Bosworth M R and Deam R T 2000 *J. Phys. D: Appl. Phys.* **33** 2605–10
[7] Deam R T, Simpson S W and Haidar J 2000 *J. Phys. D: Appl. Phys.* **33** 1393–402
[8] Shigeta M and Murphy A B 2011 *J. Phys. D: Appl. Phys.* **44** 174025
[9] Watanabe T, Atsuchi N, and Shigeta M 2007 *Thin Solid Films* **515** 4209–4216
[10] Shigeta M and Watanabe T 2007 *J. Phys. D: Appl. Phys.* **40** 2410–19
[11] Schmid H J, Al-Zaitone B, Artelt C and Peukert W 2006 *Chem. Eng. Sci.* **61** 293–305
[12] Tanaka M and Lowke J J 2007 *J. Phys. D: Appl. Phys*. **40** R1–23
[13] Tanaka M, Yamamoto K, Tashiro S, Nakata K, Yamamoto E, Yamazaki K, Suzuki K, Murphy A B and Lowke J J 2010 *J. Phys. D: Appl. Phys.* **43** 434009
[14] Mori Y, Iwao T, Yumoto M, Tashiro S and Tanaka M 2009 *Quarterly J. Japan Weld. Soc.* **27** 8s–12s (in Japanese)
[15] Tashiro S, Zeniya T, Yamamoto K, Tanaka M, Nakata K, Murphy A B, Yamamoto E, Yamazaki K and Suzuki K 2010 *J. Phys. D: Appl. Phys.* **43** 434012
[16] Tashiro S, Iwao T, Inaba T, Murphy A B and Tanaka M 2008 *IEEE Trans. Plasma Sci.* **36** 1070− 1
[17] Friedlander S K 1983 *Ann. New York Acad. Sci*. **404** 354–64
[18] Girshick S L, Chiu C P and McMurry P H 1990 *Aerosol Sci. Technol.* **13** 465–77
[19] Joshi S V, Liang Q, Park J Y and Batdorf J A 1990 *Plasma Chem. Plasma Process.* **10** 339–58
[20] Fuchs N A and Sutugin A G 1971 in "Topics in Current Aerosol Research", ed. Hidy G M and Brock J R *International Reviews in Aerosol Physics and Chemistry, Vol. 2* (Pergamon Press: New York)
[21] Borra J-P 2006 *J. Phys. D: Appl. Phys.* **39** R19–54
[22] Ounis H, Ahmadi G and Mclaughlin J B 1991 *J. Colloid Interface Sci.* **143** 266− 77
[23] Warthesen S J and Girshick S L 2007 *Plasma Chem. Plasma Process.* **27** 292–310
[24] van de Sanden M C M, Schram P P J M, Peeters A G, van der Mullen J A M and Kroesen G M W 1989 *Phys. Rev. A* **40** 5273–6